Ambient Carbon Dioxide Concentration Correlates with SARS-CoV-2 Aerostability and Infection Risk

Allen Haddrell (a.haddrell@bristol.ac.uk)
University of Bristol
Henry Oswin
University of Bristol
Mara Otero-Fernandez
University of Bristol
Joshua Robinson
Institut für Physik, Johannes Gutenberg-Universität Mainz
Tristan Cogan
University of Bristol
Robert Alexander
University of Bristol
Jamie Mann
University of Bristol https://orcid.org/0000-0001-7037-1286
Adam Finn
University of Bristol
Darryl Hill
University of Bristol
Andrew Davidson
University of Bristol
Jonathan Reid
University of Bristol https://orcid.org/0000-0001-6022-1778

Article

Keywords:

Posted Date: August 10th, 2023

DOI: https://doi.org/10.21203/rs.3.rs-3228966/v1

Abstract

An improved understanding of the underlying physicochemical properties of respiratory aerosol that influence viral infectivity may open new avenues to mitigate the transmission of respiratory diseases such as COVID-19. Previous studies have shown that a rapid increase in the pH of respiratory aerosols following generation due to changes in the gas-particle partitioning of pH buffering bicarbonate ions and carbon dioxide is a significant factor reducing viral infectivity. We show here that a significant increase in viral aerostability results from a moderate increase in the atmospheric carbon dioxide concentration (e.g. 1,800 ppm), an effect that is more marked than that observed for changes in relative humidity. We model the likelihood of COVID-19 transmission on the ambient concentration of CO_2, concluding that even a moderate increase in CO_2 concentration results in a significant increase in overall risk. These observations confirm the critical importance of ventilation and maintaining low CO_2 concentrations in indoor environments for mitigating disease transmission. Moreover, the impact of CO_2 concentration correlating with viral aerostability suggests increased risks of respiratory pathogen transmission will accompany increased ambient CO_2 concentrations as our climate changes.

Introduction

The inhalation of respiratory aerosol containing the severe acute respiratory syndrome coronavirus-2 (SARS-CoV-2) has been identified as the dominant route of transmission driving the spread of coronavirus disease 2019 (COVID-19) (1). As for all respiratory viral infections, a sufficient viral dose must be delivered to the respiratory system of an uninfected individual for disease transmission to occur. For COVID-19, this equates to inhalation of a sufficient quantity of aerosolized/inhalable and infectious SARS-CoV-2 viral particles. The minimal infectious dose is a function of many parameters, such as mucosal immunity (2), prior infection (3), and immunization status (4). Regardless of the infectious dose required, the cumulative viral load of the air inhaled will necessarily correlate with the overall risk. Thus, understanding how environmental factors affect the aerosolized viral load over time will contribute to the assessment of risk of transmission.

At their core, many of the non-pharmaceutical interventions implemented to mitigate risk of COVID-19 transmission are centered on the removal of infectious aerosolized virus from a given space. The aerosolized viral load may be altered physically by lowering the number of virus containing particles. For example, changing aerosol production rates (e.g. via singing or talking) (5, 6), crowding/social distancing policies (7), mask wearing (8), and improved ventilation (9) all reduce the total number of virus-containing aerosol droplets. The viral load within aerosol droplets may also be altered, so that the infectivity of the viral particles themselves is changed through processes such as UV germicidal irradiation (10) or by adjustments to environmental conditions such as relative humidity (RH) (11) or temperature (12). In addition to these intentional methods of disinfection, aerosolized viruses are known to lose their infectivity over time, although the precise mechanisms driving this loss remains the subject of much debate (13). A comprehensive understanding of all these processes/conditions, as well as the

interconnections between them, is necessary to facilitate the development of more effective mitigation strategies.

While many of the unique properties of aerosol have been hypothesized to play a role in the loss of viral infectivity, we have reported recently that high pH (alkaline, > 10) in respiratory aerosol surrogates is a significant contributor driving its loss (14, 15). The high pH reached by respiratory aerosol is a consequence of the mucosal liquids from which it originates (e.g. saliva, lung fluid) which contain elevated levels of bicarbonate. Following droplet generation, the pH of the neutral droplet begins to rise as the bicarbonate evaporates from the droplet in the form of gaseous carbon dioxide (CO_2) (Eq. 1):

(Eq. 1) $$H^+_{(aq)} + HCO^-_{3(aq)} \leftrightarrow H_2CO_{3(aq)} \leftrightarrow CO_{2(g)} + H_2O$$

The maximum pH the aerosol achieves, as well as the time taken to reach it, are unclear and debated (16–18). Both are a function of numerous parameters including the RH, initial aerosol droplet size, aerosol equilibrium size, initial bicarbonate concentration and ambient CO_2 concentration ($[CO_{2(g)}]$). What is clear is that models (16) and measurements (19, 20) of human exhaled aerosol have both shown consistently that exhaled respiratory aerosol is significantly more alkaline than the fluids within the respiratory tract from which they originate. Over longer time periods, the high pH of the aerosol may be neutralized through exposure to trace acidic gases, another poorly defined process that requires more investigation (17, 18). When compared to the vast majority of environmental aerosol, this pH dynamic is a peculiarity of respiratory aerosol and is critical for understanding the aerostability of respiratory viruses.

If, as reported, the pH (alkalinity) of respiratory aerosol is a major driver in the loss of viral infectivity in the aerosol phase, it can be inferred that $[CO_{2(g)}]$ has an effect on the aerostability of SARS-CoV-2 via the equilibrium described in Eq. 1. This raises three questions: over what ambient concentration range does $CO_{2(g)}$ impact infectivity, to what degree is the infectivity decay profile affected by $CO_{2(g)}$, and how does this change in infectivity affect overall risk of disease transmission?

Since 2020, CO_2 monitors have become commonly used as an indicator of potential risk of SARS-CoV-2 transmission as the $[CO_{2(g)}]$ serves as a proxy for overall ventilation efficiency and, thus, a predictor of total aerosol viral load. The source of both the aerosolized virus and CO_2 are the same (exhalation) and both are reduced through standard mitigation techniques such as ventilation (21), justifying the use of $[CO_{2(g)}]$ as a proxy indicator of transmission risk. We investigate here if elevated ambient levels of $[CO_{2(g)}]$ add a further factor to an increased transmission risk by altering the aerostability of SARS-CoV-2. This is accomplished using the Controlled Electrodynamic Levitation and Extraction of Bioaerosol onto a Substrate (CELEBS) (14, 15, 22–25) to systematically explore the effects of environmental factors such as ambient $[CO_{2(g)}]$ and RH on the aerostability of the SARS-CoV-2 Delta and Omicron variants of concern (VOC). Finally, we estimate the effect of changes in the ambient $[CO_{2(g)}]$ on the risk of transmission using the established Wells-Riley model.

Methods

Details of cell culture, viral growth, levitation assays, bulk measurements and statistical analysis is provided in the Supplementary Materials section.

Results

The BA.2 Omicron VOC is More Aero-Stable than the Delta VOC

Previously, we reported that the aerostability of the VOCs of SARS-CoV-2 (wild type, Alpha, Beta and Delta) correlated with the variant's stability in alkaline growth medium over short time periods (under five minutes) (15). Specifically, it was reported that as the virus has evolved from wild type through to Delta VOC, it has become both more sensitive to high pH and less aero-stable. The relationship between pH and the aerostability of the (Omicron) BA.2 VOC is compared to the Delta VOC to further explore this comparison (Fig. 1). Firstly, the aerostabilities of the Delta and BA.2 VOCs within aerosol droplets are reported at moderate/low (40%) and high RH (90%) values in Fig. 1A. At 40% RH, the Delta and BA.2 VOCs exhibit similar decay profiles. This is consistent with our previous studies where all VOCs exhibited a similar decay profile when the RH is below the droplet efflorescence threshold, highlighted by the near instantaneous loss of ~ 50% of viral infectivity associated with the efflorescence event. At 90% RH, the overall rate of decay of the BA.2 VOC is much slower than the Delta VOC. At 5 minutes, relative to the Delta VOC, the total percentage of viable aerosolized viral load of the BA.2 VOC is 1.7 times higher. At 90% RH, the general structures of the decay profiles for both VOCs are consistent with previous VOCs, with an initial lag period of ~ 15 seconds, followed by a rapid loss to ~ 2 minutes, and a more gradual subsequent decay.

Under high alkaline conditions in the bulk phase, the BA.2 VOC is found to be more resistant to high pH conditions than the Delta VOC assessed via two different measurements of infectivity (Figs. 1B and 1C). This is consistent with the hypothesis that the differences between aerostability of the Delta and BA.2 VOCs are likely a consequence of their relative stability in a highly alkaline solution. BA.2 is the first VOC of SARS-CoV-2 that we have demonstrated to have an increase in stability at high pH when compared to a previous VOC. The microbiological mechanisms underlying these differences in pH sensitivity remain unclear and are in need of further research.

Collectively, the data shown in Fig. 1 support the hypothesis that high pH achieved in aerosol, with an initial composition that has high abundance of bicarbonate (such as saliva (26) and growth medium), is a major factor in driving loss of viral infectivity in the aerosol phase (15). The implication of this proposed mechanism is that any gaseous species (e.g., CO_2) that can affect aerosol pH is likely to impact viral infectivity.

SARS-CoV-2 Aerostability Correlates with the Ambient Concentration of Gas Phase Carbon Dioxide

In poorly ventilated, occupied, indoor spaces, ambient [$CO_{2(g)}$] commonly reaches concentrations exceeding 2,000 ppm (27) and can reach levels upwards of > 5,000 ppm in more crowded environments (28). The impact of elevated $CO_{2(g)}$ levels on the aerostability of SARS-CoV-2 is explored (Fig. 2). The maximum titre of the BA.2 VOC that can be grown in the cell culture is approximately an order of magnitude less than that of the Delta VOC. Both the sensitivity and the throughput of the CELEBS technique are dependent on the initial viral load of the individual droplets. Thus, in order to explore the effect that [$CO_{2(g)}$] has on viral aerostability across a broad range of conditions and over very long time periods, only the Delta VOC was used, as it afforded a much higher measurement throughput.

When compared to a typical atmospheric [$CO_{2(g)}$] (~ 500 ppm), any increase in the [$CO_{2(g)}$] results in a significant increase in viral aerostability after 2 minutes (Fig. 2A). When ambient air flow into the CELEBS was substituted with compressed (CO_2 free) air, no change in virus aerostability was observed. It is notable that whilst the increase in [$CO_{2(g)}$] to ~ 6,500 ppm resulted in a more significant increase in aerostability, it did not result in complete stabilization of virus in the aerosol phase (Fig. 2A).

With the rate of loss of viral infectivity increased by elevated aerosol alkalinity, any improvement in aerostability of SARS-CoV-2 resulting from elevated [$CO_{2(g)}$] would be expected to increase over time with a greater tendency towards neutral pH due to the dissolution of carbonic acid. The effect of droplet exposure to elevated [$CO_{2(g)}$] over prolonged time periods on the infectious viral load is reported in Fig. 2B and it can be seen that elevated [$CO_{2(g)}$] had a considerable effect on the overall decay profile. Consider first the characteristics of the decay profile of the wild type SARS-CoV-2 in the aerosol phase above the efflorescence point (14). From droplet generation until ~ 2 minutes, no loss of infectivity is observed. After 2 minutes there is a rapid loss of infectivity over a moderate time-period (minutes), followed by a slower decay (tens of minutes). The profile for the Delta VOC is similar, but with the initial lag period shortened to ~ 15 seconds. In this case, when the [$CO_{2(g)}$] is elevated, the period of rapid decay is absent or greatly abbreviated and the decay profile transitions directly from lag to a slow decay. As a result, the Delta VOC in elevated [$CO_{2(g)}$] is as aero-stable as the wild type at 500 ppm CO_2 after 5 minutes, becoming more stable after 20 minutes. Indeed, an elevated [$CO_{2(g)}$] had a dramatic effect on the remaining relative infectivity of SARS-CoV-2 over time (Fig. 2C). After 40 minutes, approximately an order of magnitude more viral infectious units remained viable in the aerosol phase at elevated [$CO_{2(g)}$] when compared to the loss expected under ambient (well ventilated) conditions. This increase in the relative abundance of infectious particles is likely to result in increased risk of transmission of the infection.

Viral aerostability is often reported as having a half-life (29) with the decay assumed to follow first order (exponential) reaction kinetics. This assumption presupposes that the mechanisms involved in infectivity loss do not change over time, even though the chemical composition and physical conditions inside an aerosol droplet vary over time. The appropriateness of making such assumptions is explored in Fig. 2D. In the bulk phase, the pH driven decay follows first order kinetics. This is consistent with high [OH^-] driving the loss of viral infectivity, with this concentration remaining constant over time. However, the decay dynamics are markedly different in the aerosol phase with the rate of loss slowing over time, and slowing

more so at higher [$CO_{2(g)}$]. This is consistent with the hypothesis that the aerosol reaches high pH before being buffered towards a neutral pH by trace acidic vapor over longer time periods (condensable carbonic acid in this case), regardless of RH. However, the decay rate is never found to increase over the entire time-period studied, suggesting that the pH of the aerosol does not pass through neutral to become acidic during the time period when more than 95% of the viral infectivity is lost. Again, this is consistent with the condensation of a weak acid, carbonic acid in this case. However, an estimate of a half-life of ~ 80 minutes could be estimated from the data falling between 20 and 40 minutes at [$CO_{2(g)}$] of 3,000 ppm if one were to assume a first order decay. This aligns with the half-lives reported for systems in which the [$CO_{2(g)}$] is neither measured nor controlled (29).

Collectively, the data shown in Fig. 2 show that the interplay between aerosol alkalinity and CO_2 has a profound effect on the overall aerostability of SARS-CoV-2. Any increase in [$CO_{2(g)}$] results in an increase in aerostability.

Depending on Variant pH Sensitivity, Ambient [CO_2] and Solute Composition Can Affect Viral Aerostability More than Relative Humidity

During the COVID-19 pandemic, many infections were traced to super-spreader events (30), suggesting that transmission of the virus over longer distances was possible under some (as yet uncertain) conditions. Conversely, the apparent effectiveness of mitigation strategies such as social distancing regulations (7), use of face shields/masks (31) and installation of plexiglass shields (32) suggests that SARS-CoV-2 was also commonly transmitted over short distances. Thus, it is important to understand how environmental factors affect the aerostability of SARS-CoV-2 over time periods as short as 15 seconds.

Fixing the time in the aerosol phase at 15 seconds, the BA.2 VOC is found to be more aero-stable than the Delta VOC across a broad range of RH (Fig. 3A). Effectively, during the first 15 seconds post-aerosol generation there is no loss of infectivity of the BA.2 VOC when the RH is above the efflorescence point of the particle (RH ~ 50%). Below that, the characteristic rapid loss of approximately half of the viral infectivity is observed, a consequence of the efflorescence event. This is consistent with the loss observed for the others SARS-CoV-2 VOC we have studied (14, 15, 33) as well as for mouse hepatitis virus (MHV), another coronavirus (34). However, the Delta VOC rapidly loses over half of its infectivity within 15 seconds of being in the aerosol phase, regardless of RH (below 90%) and across a broad range. Collectively, the data in Fig. 3A show that the initial decay of the Delta VOC is largely RH independent, while the initial decay of the BA.2 VOC is highly RH dependent.

Given that the BA.2 VOC is more robust than the Delta VOC over the 15 s time period, the impact of [$CO_{2(g)}$] and [NaCl] on the aerostability of the Delta VOC have been explored further. The effect that a moderate increase in [$CO_{2(g)}$] has on the aerostability of this SARS-CoV-2 VOC is reported in Fig. 3B. Regardless of RH, increasing the [$CO_{2(g)}$] will drive the pH of an alkaline respiratory droplet towards neutral to some degree. As a result, at an RH of 80% and below, moderate increases in the [$CO_{2(g)}$] are

shown to increase viral aerostability. This increase in [$CO_{2(g)}$] results in a doubling of the remaining aerosolized viral load after 15 s, regardless of RH.

The solute composition of saliva between individuals may vary widely. Moreover, an individual's salivary [NaCl], as well as the ratio of NaCl to other solutes, may vary dramatically as a result of short-term events, such as oral stimulation (35), or larger physiological changes, such as pregnancy (36). The effect that altering the initial [NaCl] of the starting formulation on the short term aerostability is reported in Fig. 3C.

We previously reported that the fraction of SARS-CoV-2 in a particle that resides in the salt crystal following the efflorescence event is shielded and thus remains infectious. Accordingly, any observed increase in sustained infectivity below an RH of 50% can be attributed to the increase in the volume of the particle that forms a solute salt crystal. The same trend is observed in Fig. 3C: the addition of NaCl results in a significant increase in sustained aerostability at RHs below 50%. Between the RHs of 50% and 75%, we previously reported that the physical structures of MEM droplets is complex with phase structures across a population of droplets that are a mixture of a homogeneous liquid droplet form and liquid droplets containing a suspension (e.g. emulsion or salt crystals) (14). When the [NaCl] is doubled, the proportions across a population is such that all particles undergo a phase change when the RH is below ~ 75% (Supplemental Fig. 1). Accordingly, the crystalline form offers protection to the virus when the RH is below ~ 75% and this protection is more pronounced when the [NaCl] is doubled. Hence, the remaining fraction of infectious virus remains higher across all RHs below 75%. At 80% RH, no phase change is observed and the increase of [NaCl] has no effect on the viral aerostability.

Risk of Transmission is Highly Affected by Ambient Concentrations of CO

The dependence of the overall risk of SARS-CoV-2 transmission on the explicit decay dynamics inferred from measurements with the CELEBS technique has been investigated using a Wells-Riley model (37). The effects that environmental factors such as [$CO_{2(g)}$] and humidity on the likelihood of disease transmission have been explored. The Wells-Riley model is based on transmitted quanta that inherently assume a uniformly mixed room ("gas" phase like), which is only true for small particles largely in bronchiolar and laryngeal mode, both < 5 μm diameter. The decay data measured in this study are for droplet sizes in the oral mode (initially > 50 μm diameter). We use the infectivity decay data from these large droplet measurements to inform estimates of transmission risk for the small aerosol fraction and to estimate the relative changes in risk that result from changes in [$CO_{2(g)}$].

Typically, models assume that the aerosolized viral decay has a half-life of 1.1 hours (38) when estimating the risk of COVID-19 transmission, a rate of decay which is negligible when compared to the effects of even the poorest ventilation. As shown in Fig. 1, viral decay dynamics are more complex than the assumed single exponential decay. Moreover, the rapid early decay in infectivity of aerosolized SARS-CoV-2 we report here, as well as previously (14), appears to contradict the consensus opinion that

airborne transmission prevails as the dominant mode of transmission. However, our objective here is to demonstrate that the decay dynamics reported in Figs. 1A and 2B are actually consistent with this consensus, especially in indoor environments. We therefore focus on the limit of a well-mixed indoor environment using the Wells-Riley framework and using our refined characterization of the infectivity decay rate.

Central to the Wells-Riley approach is the number of infectious units ("quanta") that remain active in a room. In a ventilated environment, the probability that an aerosolized unit remains in the room after some time is described by Eq. 2.

$$\textbf{(Eq. 2):} p_{active} = 1 - exp\left(\frac{-t}{\tau_{vent}}\right)$$

where τ_{vent} is the characteristic time to cycle air in the room. We consider typical ventilation rates for τ_{vent}^{-1} in the range 0.5–8 hr^{-1} with smaller numbers indicating a poorly ventilated space (39). Any effect of droplet removal by deposition which may occur for coarser droplets is ignored. The fraction of droplets remaining viable to initiate infection is $p_{active}I$, where *I* is their infectivity. Initially we consider ventilation within a fully recirculating system where the [$CO_{2(g)}$] remains constant so that we can assume the decay in infectivity directly follows that reported from the CELEBS data; this set-up models a closed Heating, Ventilation and Air-Condition (HVAC) system. We assume the HVAC system perfectly filters the air of aerosol droplets, although this is a crude oversimplification (40). Later we will allow for varying [$CO_{2(g)}$] in order to model ventilation and mixing with an outdoor air source (from e.g. opening a window). For convenience we fit the CELEBS data (Figs. 1A and 2B) with two exponentially decaying functions (details in Supplementary). In poorly ventilated environments, the viability of aerosolized virus is dominated by the intrinsic decay in infectivity (Fig. 4A). Air recirculation dominates in better conditioned environments leading to convergence of the long-time decay (Fig. 4B). We compare these model predictions with a simple exponentially decaying infectivity with the widely assumed aerosolized half-life of 1.1hr (29).

In the Wells-Riley model, the infection probability p_I is assumed to depend exponentially on the number of infectious units ("quanta") received n, i.e. $p_I(t) = 1 - exp(-n(t))$. This is essentially a consequence of the independent action hypothesis (41). The typical number of quanta received increases linearly in time t as $n(t) = c\,\dot{V}\,t$ where c is the concentration of quanta in the well-mixed air and $\dot{V}$ is the minute volume of exhaled air (from breathing) which we take to be 7.5 L/min. The steady state quanta concentration is found where $p_{active}I$ balances the rate that infectious quanta are produced and released into the environment (details in Supplementary). For illustration purposes, we consider a 10×10×3=300 m^3 classroom with up to 40 occupants where there is a single infected individual. The quanta production rate by an infected individual is considered to be in the range 0.01–0.1 s^{-1} for SARS-CoV-2 (38). We assume a value of 0.1 s^{-1} for illustrative purposes, with the understanding that this factor remains a major source of uncertainty in transmission models. The probability of onwards transmission

in a poorly ventilated classroom is similar for all datasets at low [$CO_{2(g)}$] (Fig. 4C), because only the long-time behavior matters in this well-mixed limit. By contrast, the probability of onwards transmission rises much more rapidly for the high [$CO_{2(g)}$]. The amplifying effect of [$CO_{2(g)}$] is visible but less pronounced in a space with good ventialtion using e.g. an open window (Fig. 4D).

For risk management we must consider the risk that *any* susceptible individual becomes infected, rather than just a single individual. The probability that at least one individual becomes infected is:

(Eq. 3): $$1-\left(1-p_I\left(t\right)\right)^{N-1}$$

where N is the room occupancy. As a measure of risk, we invert this relationship to determine the length of time the classroom space can be shared until there is a 50% chance that secondary transmission has occurred. The probability of a successful transmission (assuming a well-mixed environment) as a function of viral aerostability and ventilation is explored in Fig. 5. Estimates for the Delta variant at high [$CO_{2(g)}$] are comparable in magnitude to predictions with a decay time assumed from the drum studies. Moreover, the [$CO_{2(g)}$] is estimated to have a profound effect on overall risk both in terms of room occupancy and ventilation rates.

Sustained [$CO_{2(g)}$] at a higher concentration at a fixed ventilation rate (e.g. more recirculation of room air and less mixing of fresh air) means lower aerosol pH, means greater survival means shorter time until 50% transmission. Assuming a slower decay consistent with the drum data does not incorporate the rapid initial loss of infectivity which means at the same quanta emission rate, there is more infectious virus and shorter time to reach 50% infectivity. Outdoor air, lowers the CO2 concentration, mixing in low CO2 fresh air, that means the pH remains higher, means lower infectivity, means longer time to reach same infectivity as ACH goes up.

Despite the rapid initial decay (Figs. 1A and 2B), the Wells-Riley model prediction estimates that long distance transmission is possible. However, the Wells-Riley model neglects short-time decay indicating that short-range airborne transmission route (from e.g. direct conversation) may be underestimated in these conventional approaches. Collectively, the risk estimations from the Wells-Riley model demonstrate the importance of ventilation in mitigating risk as it addresses aerosolized viral load on two fronts: firstly, the rate of loss of viral infectivity in the aerosol phase (e.g. lower [$CO_{2(g)}$] increases decay rate) and, secondly, the physical reduction of the number of viral containing particles (e.g. displaced from the room). The Wells-Riley model demonstrates the importance of [$CO_{2(g)}$] and RH on long distance transmission risk. In the future, the effect the rapid loss of infectivity in the aerosol phase at low RH has on short distance transmission risk should be explored using a CFD model.

Discussion

In the absence of infectious virus sampling, ambient [$CO_{2(g)}$] has been shown to indicate increased COVID-19 infection risk, through a reduction in effective ventilation and an increase in infectious particle

concentrations (42). The data presented here suggests that [$CO_{2(g)}$] concentration may be more than just an indicator of poor ventilation or air filtration efficiency. Ultimately the aerosolized virus and CO_2 have the same origin, and their mutual interaction increases the overall risk (Fig. 5). This means that the utility of [$CO_{2(g)}$] as a proxy for transmission is of increased value as increased [$CO_{2(g)}$] itself may increase the likelihood of successful transmission by increasing viral viability.

Broader Implications

The ability of [$CO_{2(g)}$] to affect virus aerostability may have broader implications beyond disease transmission, and prompts many new avenues of research. For example, the aerostability of a virus being affected by the [$CO_{2(g)}$] raises many questions regarding the potential effect that increases in the [$CO_{2(g)}$] in the atmosphere has on both the transmissibility of extant viruses, as well as on the emergence of novel viruses. [$CO_{2(g)}$] has increased from preindustrial revolution (275 ppm), through to now (~ 400 ppm), and may reach upwards of > 1,000 ppm by the turn of the century (43). This increase may be enough to improve viral transmission through both increasing the aerostability of the virus outdoors, but also increasing the baseline [$CO_{2(g)}$] indoors as well.

Respiratory viral infections, such as influenza and rotavirus, are notable as they have a seasonality (44). There are numerous hypotheses as to what drives this process including, for example, that the dry indoor air over winter may have an effect (45, 46). The effect of RH may also be important with regards to processes such as mucosal immunity (2, 47) and plume dynamics (48), and less so for the viral infectivity. Seasonal variation in indoor [$CO_{2(g)}$] occurs globally, across a broad range of geographies (49–51). From the experimental and model data reported here, we hypothesize that the seasonality of respiratory viral infections at a populations scale may be affected by indoor [$CO_{2(g)}$] as well as changes in RH. Further study is needed to explore this relationship across a broad range of respiratory viruses.

Moderate increases in [$CO_{2(g)}$] affecting the aerostability of SARS-CoV-2 have very broad implications with regards to how all previously published aerovirology experiments should be interpreted. Standard experiments involve the nebulization of a virus-containing starting formulation into a confined volume where the aerosol is suspended. The starting formulation will contain some level of bicarbonate, either from the growth medium in which the virus is made, or because the starting formulation is some form of respiratory fluid. If the starting formulation does not have bicarbonate, the utility of the data is questionable as the starting formulation is missing a critical component that is both driving the loss of viral infectivity in respiratory aerosol and necessarily a part of the respiratory system of mammals. The presence of bicarbonate in the starting formulation necessitates that CO_2 must be produced during the nebulization process, and there is no physical means to separate the aerosol condensed phase from the gas phase. The amount of CO_2 produced will be a product of the nebulization time (14). A survey of the literature found that a large portion of manuscripts do not provide the nebulization period, while none have been found to report the [$CO_{2(g)}$]. Accordingly, in the study of aerosolized viruses, a major parameter that affects viral aerostability (CO_2) is simultaneously intrinsic in the experiment, and not considered.

The decay rate of SARS-CoV-2 in aerosol as measured with a rotating drum, or similar closed system in which the sample is nebulized and the subsequent plume was captured, is reported as a half-life of ~ 1.1 hours (10, 11, 29). This matches with the half-life reported in this study when the [$CO_{2(g)}$] was elevated (Fig. 2D, after 20 minutes). Direct confirmation of this is not possible as the [$CO_{2(g)}$] in rotating drum studies have never been reported. In the absence of elevated [$CO_{2(g)}$], the half-life as measured with the CELEBS for any of the SARS-CoV-2 VOCs is < 20 minutes. The ability for small increases in [$CO_{2(g)}$] to dramatically increase the aerostability of SARS-CoV-2 largely explains the discrepancy between the aerostability reported using the CELEBS system with those reported previously using nebulized based instruments.

SARS-CoV-2 has a Triphasic Decay Profile

The high time resolution of the CELEBS technology has afforded unique insights into the decay dynamics of aerosolized viruses that have been previously impossible. Historically, the decay of an aerosolized virus has been described as having a half-life. As shown here and in previous studies (14, 15, 25), this is clearly not the case (Fig. 2D). Rather, the decay profile is a complex process that is highly dependent on both microbiology and aerosol dynamics. From our studies using this next generation technology, we have found that there are 3 distinct phases of aerosolized viral decay: the Lag Phase, the Dynamic Phase and the Slow Decay Phase as shown schematically in Fig. 6.

First is the “Lag Phase”. During this phase, the conditions in the droplet are in flux (i.e. CO_2 evaporation, water evaporation, solute concentration), but the conditions are such that they are not yet toxic to the viral particle. The length of the Lag Phase is highly RH (Fig. 3A), temperature, [$CO_{2(g)}$] (Fig. 3B) and variant dependent (Fig. 2B). At low RH, the Lag Phase is very short (< 5s) since droplet efflorescence will initiate rapid loss of viral infectivity (Fig. 5, Top). At high RH, the pH of the droplet increases during the Lag Phase, thus the time before the virus begins to decay is dependent on how sensitive the virus is to pH (Figs. 1A and 3A), and the speed at which the aerosol pH rises (Figs. 3B), a process that may take on the order of minutes. The wild type SARS-CoV-2 had a 2 minute Lag Period. The virus was readily able to survive the rapid increase in salt concentration that took place over the first 20–30 seconds of aerosolization. Viral decay did not begin until the pH level had considerably increased when it began to drive the loss of infectivity (Fig. 6D). It is likely that the increase in salt concentration plays a role in further increasing the rate of viral inactivation but based on the length of the Lag Period relative to the evaporation rate, we suggest that the change in salt concentration alone is not the primary driving force. The interplay between these two processes on viral stability needs to be explored further.

After the Lag Phase, the conditions in the droplet are still in flux, while the pH increase is still occurring. The second phase of decay is the “Dynamic Phase” phase. In this phase, the pH in the droplet have changed to the point where they have become toxic to the virus and the rate of loss is dictated by the changing conditions in the droplet. For example, the rapid loss of infectivity during efflorescence may occur in the Dynamic Phase.

The final phase is the “Slow Decay Phase” phase where the loss of viral infectivity is much slower than the Dynamic Phase. The Slow Decay Phase continues until all viral infectivity is lost, which may take tens of minutes to hours, depending on the virus and environmental conditions. The mechanism of the slower decay rate in this phase remains unclear and may be biological (e.g. fraction of strain being more resilient to the conditions) or physical/chemical (e.g. the remaining virus protected by its immediate location such as in a liposome or associated with a protein (25)). The length of the Lag Period, and the rate of loss in the Dynamic Phase are both highly dependent on the pH sensitivity of the virus as well as $[CO_{2(g)}]$ and RH. At a high $[CO_{2(g)}]$, the Dynamic Phase can be dramatically truncated or even eliminated entirely (Fig. 2B). The decay rate in the Slow Decay Phase is largely RH independent, but highly dependent on the $[CO_2]$ (Figs. 2A, 2B, 2D and 3B). The data collected using closed systems, such as a Goldberg drum, largely miss the Lag and Dynamic phases (perhaps catching the tail end of the Dynamic Phase), and measure primarily in the Slow Decay Phase. Moreover, the rate of loss in the Slow Decay Phase is highly $[CO_{2(g)}]$ dependent (Figs. 2A, 2B, 2D and 3B).

The Triphasic Viral Aerosol Decay (TVAD) profile accurately describes the general relationship between viral infectivity and aerosolization time. The applicability of the TVAD to all other respiratory viruses is unclear, though it is notable that we have observed similar behaviour for the MHV virus and all VOC for SARS-CoV-2 (14, 25, 34). It provides a framework to understand and explore which properties of the viral particle or the aerosol droplet will affect the likelihood of both short and long distance transmission. The parameters that affect the Lag and Dynamic phases may affect short distance transmission while the parameters that effect the Slow Decay Phase may affect long distance transmission.

Declarations

Acknowledgements

Vero E6 cells modified to stably express human ACE2 and TMPRSS2 were a kind gift from Dr Suzannah Rihn, MRC-University of Glasgow Centre for Virus Research. Viral stocks of the B.1.617.2 (Delta) (GISAID ID: EPI_ISL_1731019) and Omicron (BA.2) VOCs were kindly provided by Professor Wendy Barclay, Imperial College, London, Professor Maria Zambon, UK Health Security Agency, and Dr Thushan de Silva, University of Sheffield. This work was funded by: the National Institute for Health Research-UK Research and Innovation (UKRI) rapid COVID-19 call, the Elizabeth Blackwell Institute for Health Research, the University of Bristol, and the Medical Research Council, the PROTECT COVID-19 National Core Study on transmission and environment, managed by the Health and Safety Executive on behalf of Her Majesty’s Government. The EPSRC Centre for Doctoral Training in Aerosol Science EP/S023593/1 which supported R.A. and J.T is acknowledged. A.E.H. and M.O.-F. received funding from the Biotechnology and Biological Sciences Research Council (BB/W00884X/1). J.F.R. is supported by funding from the Alexander von Humboldt foundation. A.D.D. is a member of the G2P-UK National Virology consortium funded by the Medical Research Council/UKRI (Grant MR/W005611/1) that supplied SARS-CoV-2 variants. H.P.O. is supported by funding from the Defence Science and Technology Laboratory and the Engineering and

Physical Sciences Research Council. S.J.C is supported by the Leverhulme Trust (Early Career Fellowship, ECF-2021-072) and the Isaac Newton Trust (20.08(r)). The authors would also like to acknowledge the critical role that the Bristol UNCOVER Group played in organizing this collaboration.

References

1. D. Duval *et al.*, Long distance airborne transmission of SARS-CoV-2: rapid systematic review. BMJ 377, e068743 (2022).
2. M. W. Russell, Z. Moldoveanu, P. L. Ogra, J. Mestecky, Mucosal Immunity in COVID-19: A Neglected but Critical Aspect of SARS-CoV-2 Infection. Front Immunol 11, 611337 (2020).
3. C.-F. Team, Past SARS-CoV-2 infection protection against re-infection: a systematic review and meta-analysis. Lancet 401, 833–842 (2023).
4. N. Bobrovitz *et al.*, Protective effectiveness of previous SARS-CoV-2 infection and hybrid immunity against the omicron variant and severe disease: a systematic review and meta-regression. The Lancet Infectious Diseases 23, 556–567 (2023).
5. J. Archer *et al.*, Comparing aerosol number and mass exhalation rates from children and adults during breathing, speaking and singing. Interface Focus 12, (2022).
6. F. K. A. Gregson *et al.*, Comparing aerosol concentrations and particle size distributions generated by singing, speaking and breathing. Aerosol Sci Tech 55, 681–691 (2021).
7. U. Glogowsky, E. Hansen, S. Schächtele, How effective are social distancing policies? Evidence on the fight against COVID-19. Plos One 16, e0257363 (2021).
8. G. Tanisali *et al.*, Effectiveness of different types of mask in aerosol dispersion in SARS-CoV-2 infection. Int J Infect Dis 109, 310–314 (2021).
9. G. M. Thornton *et al.*, The impact of heating, ventilation, and air conditioning design features on the transmission of viruses, including the 2019 novel coronavirus: A systematic review of ventilation and coronavirus. PLOS Global Public Health 2, e0000552 (2022).
10. M. Schuit *et al.*, Airborne SARS-CoV-2 Is Rapidly Inactivated by Simulated Sunlight. J Infect Dis 222, 564–571 (2020).
11. S. J. Smither, L. S. Eastaugh, J. S. Findlay, M. S. Lever, Experimental aerosol survival of SARS-CoV-2 in artificial saliva and tissue culture media at medium and high humidity. Emerg Microbes Infec 9, 1415–1417 (2020).
12. C. Batéjat, Q. Grassin, J. C. Manuguerra, I. Leclercq, Heat inactivation of the severe acute respiratory syndrome coronavirus 2. J Biosaf Biosecur 3, 1–3 (2021).
13. C. C. Wang *et al.*, Airborne transmission of respiratory viruses. Science 373, eabd9149 (2021).
14. H. P. Oswin *et al.*, The dynamics of SARS-CoV-2 infectivity with changes in aerosol microenvironment. Proc Natl Acad Sci U S A 119, e2200109119 (2022).
15. A. Haddrell *et al.*, Differences in airborne stability of SARS-CoV-2 variants of concern is impacted by alkalinity of surrogates of respiratory aerosol. J R Soc Interface 20, 20230062 (2023).

16. B. Luo *et al.*, Acidity of expiratory aerosols controls the infectivity of airborne influenza virus and SARS-CoV-2. Environ Sci Technol 57, 486–497 (2022).
17. L. K. Klein *et al.*, Expiratory aerosol pH is determined by indoor room trace gases and particle size. Proc Natl Acad Sci U S A 119, e2212140119 (2022).
18. H. P. Oswin *et al.*, Reply to Klein et al.: The importance of aerosol pH for airborne respiratory virus transmission. *Proc Natl Acad Sci U S A* 119, e2212556119 (2022).
19. K. Kostikas *et al.*, pH in expired breath condensate of patients with inflammatory airway diseases. Am J Resp Crit Care 165, 1364–1370 (2002).
20. J. Vaughan *et al.*, Exhaled breath condensate pH is a robust and reproducible assay of airway acidity. Eur Respir J 22, 889–894 (2003).
21. A. Di Gilio *et al.*, CO2 concentration monitoring inside educational buildings as a strategic tool to reduce the risk of Sars-CoV-2 airborne transmission. Environ Res 202, (2021).
22. M. O. Fernandez *et al.*, Assessing the airborne survival of bacteria in populations of aerosol droplets with a novel technology. J R Soc Interface 16, (2019).
23. M. O. Fernandez, R. J. Thomas, H. Oswin, A. E. Haddrell, J. P. Reid, Transformative Approach To Investigate the Microphysical Factors Influencing Airborne Transmission of Pathogens. Appl Environ Microb 86, (2020).
24. H. P. Oswin *et al.*, Oxidative Stress Contributes to Bacterial Airborne Loss of Viability. Microbiol Spectr, e0334722 (2023).
25. R. W. Alexander *et al.*, Mucin Transiently Sustains Coronavirus Infectivity through Heterogenous Changes in Phase Morphology of Evaporating Aerosol. Viruses 14, 1856 (2022).
26. A. Bardow, J. Madsen, B. Nauntofte, The bicarbonate concentration in human saliva does not exceed the plasma level under normal physiological conditions. Clin Oral Investig 4, 245–253 (2000).
27. S. Bogdanovica, J. Zemitis, R. Bogdanovics, The Effect of CO2 Concentration on Children's Well-Being during the Process of Learning. Energies 13, 6099 (2020).
28. C.-F. Chiu, M.-H. Chen, F.-H. Chang, Carbon Dioxide Concentrations and Temperatures within Tour Buses under Real-Time Traffic Conditions. Plos One 10, e0125117 (2015).
29. N. van Doremalen *et al.*, Aerosol and Surface Stability of SARS-CoV-2 as Compared with SARS-CoV-1. N Engl J Med 382, 1564–1567 (2020).
30. D. Majra, J. Benson, J. Pitts, J. Stebbing, SARS-CoV-2 (COVID-19) superspreader events. J Infect 82, 36–40 (2021).
31. G. Leech *et al.*, Mask wearing in community settings reduces SARS-CoV-2 transmission. Proc Natl Acad Sci U S A 119, e2119266119 (2022).
32. J. J. Herstein *et al.*, Characteristics of SARS-CoV-2 Transmission among Meat Processing Workers in Nebraska, USA, and Effectiveness of Risk Mitigation Measures. Emerg Infect Dis 27, 1032–1038 (2021).

33. P. A. Dabisch *et al.*, Comparison of the survival of different isolates of SARS-CoV-2 in evaporating aerosols. Aerosol Sci Tech, 1–12 (2022).
34. H. P. Oswin *et al.*, Measuring stability of virus in aerosols under varying environmental conditions. Aerosol Sci Tech 55, 1315–1320 (2021).
35. C. Dawes, The effects of flow rate and duration of stimulation on the condentrations of protein and the main electrolytes in human parotid saliva. Arch Oral Biol 14, 277–294 (1969).
36. T. J. Lasisi, P. N. Ugwuadu, Pregnancy related changes in human salivary secretion and composition in a Nigerian population. Afr J Med Med Sci 43, 347–351 (2014).
37. E. C. Riley, G. Murphy, R. L. Riley, Airborne Spread of Measles in a Suburban Elementary School. American Journal of Epidemiology 107, 421–432 (1978).
38. M. Z. Bazant, J. W. M. Bush, A guideline to limit indoor airborne transmission of COVID-19. Proc Natl Acad Sci U S A 118, (2021).
39. T. Lipinski, D. Ahmad, N. Serey, H. Jouhara, Review of ventilation strategies to reduce the risk of disease transmission in high occupancy buildings. International Journal of Thermofluids 7–8, 100045 (2020).
40. G. H. Downing *et al.*, Computational and experimental study of aerosol dispersion in a ventilated room. Aerosol Sci Tech 57, 50–62 (2023).
41. M. P. Zwart *et al.*, An experimental test of the independent action hypothesis in virus-insect pathosystems. Proc Biol Sci 276, 2233–2242 (2009).
42. P. Z, J. JL, - Exhaled CO(2) as a COVID-19 Infection Risk Proxy for Different Indoor. - *Environ Sci Technol Lett. 2021 Apr 5:acs.estlett.1c00183. doi:*, T - epublish.
43. W. Cheng *et al.*, Global monthly gridded atmospheric carbon dioxide concentrations under the historical and future scenarios. Sci Data 9, 83 (2022).
44. M. Moriyama, W. J. Hugentobler, A. Iwasaki, Seasonality of Respiratory Viral Infections. Annu Rev Virol 7, 83–101 (2020).
45. J. E. Park *et al.*, Effects of temperature, humidity, and diurnal temperature range on influenza incidence in a temperate region. Influenza Other Respir Viruses 14, 11–18 (2020).
46. A. C. Lowen, J. Steel, Roles of Humidity and Temperature in Shaping Influenza Seasonality. J Virol 88, 7692–7695 (2014).
47. E. Kudo *et al.*, Low ambient humidity impairs barrier function and innate resistance against influenza infection. P Natl Acad Sci USA 116, 10905–10910 (2019).
48. H. Li *et al.*, Airborne dispersion of droplets during coughing: a physical model of viral transmission. Sci Rep-Uk 11, 4617 (2021).
49. R. Abdelnabi *et al.*, Comparing infectivity and virulence of emerging SARS-CoV-2 variants in Syrian hamsters. Ebiomedicine 68, (2021).
50. S. Deng, J. Lau, Seasonal variations of indoor air quality and thermal conditions and their correlations in 220 classrooms in the Midwestern United States. Build Environ 157, 79–88 (2019).

51. M. Elbayoumi, N. A. Ramli, N. F. F. Md Yusof, W. A. Madhoun, The effect of seasonal variation on indoor and outdoor carbon monoxide concentrations in Eastern Mediterranean climate. Atmospheric Pollution Research 5, 315–324 (2014).

Figures

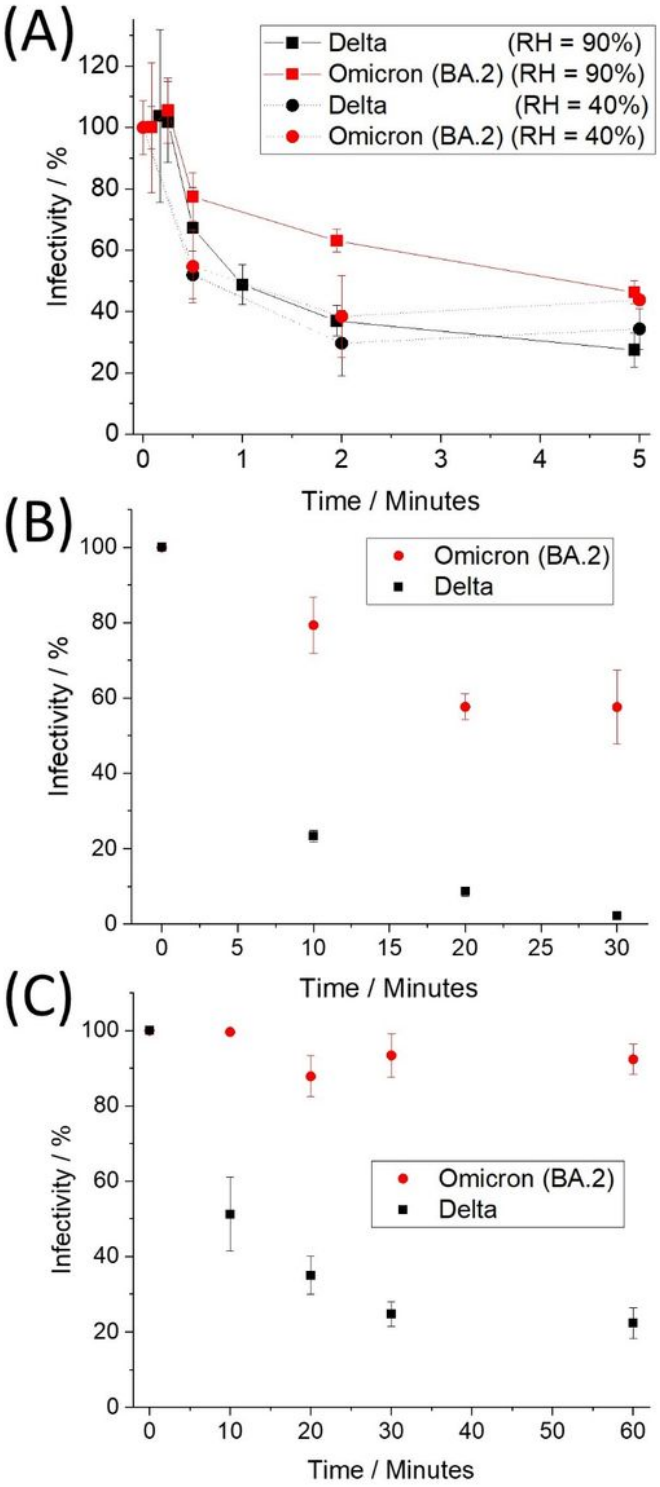

Figure 1

(A) Infectivity of the Delta and Omicron BA.2 VOCs that have been levitated at RHs of 40% and 90%. Data for 90% at times over 100s are offset by 5s to facilitate reader interpretation. BA.2 and Delta VOCs in DMEM 2% FBS bulk solution with pH maintained at 11 and infectivity measured by (B) cytopathy and (C) immunostaining. Error bars indicate standard error for all figures.

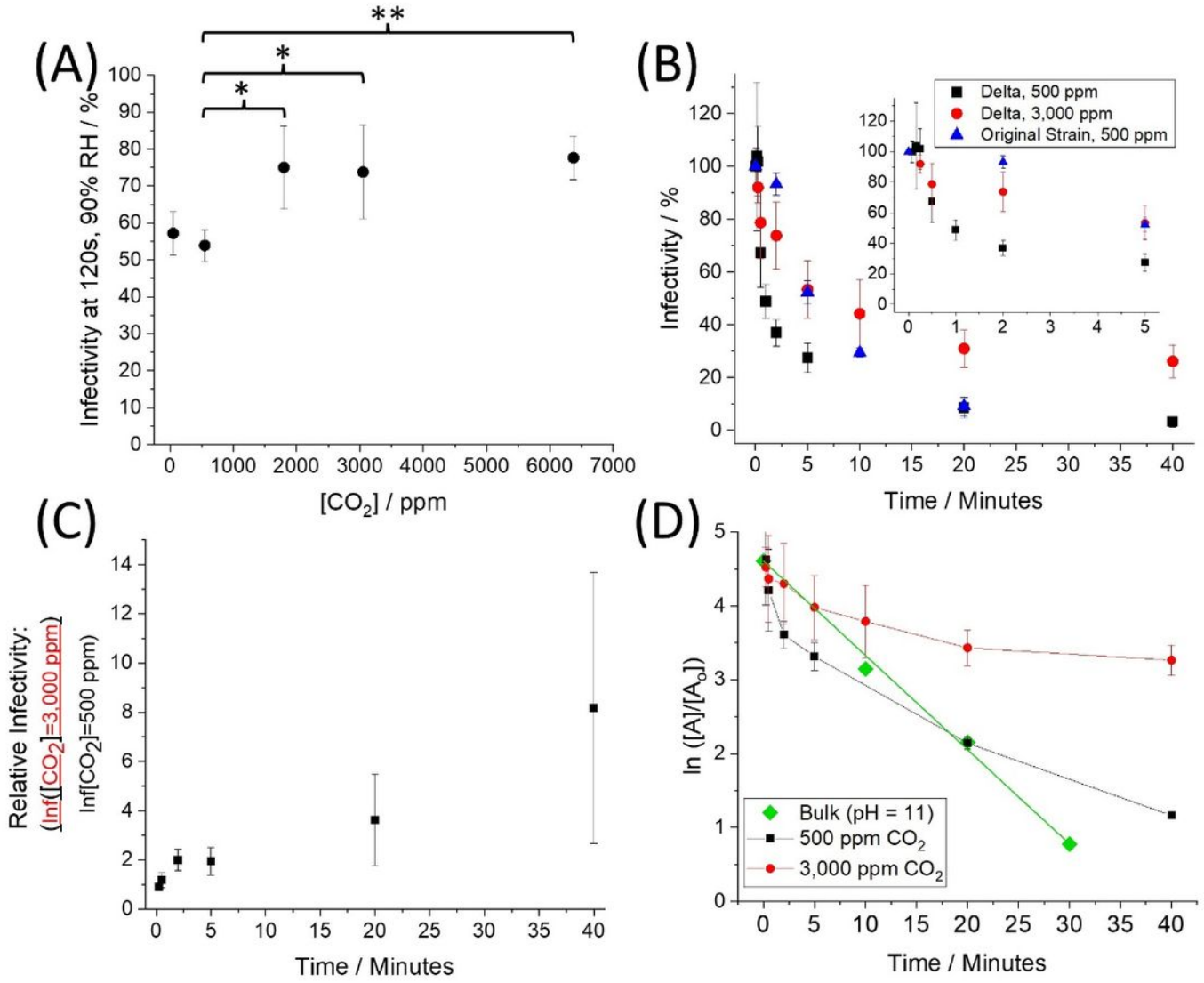

Figure 2

Exploring the effect that $[CO_{2(g)}]$ has on the aerostability of the Delta VOC as measured with the CELEBS. (A) Infectivity as a function of ambient concentrations of CO_2. Statistical significance was assessed using a two-sample equal-variance t-test (*$p \leq 0.05$, **$p \leq 0.005$). (B) The effect that an elevated concentration of CO_2 has on the decay profile of the Delta variant of SARS-CoV-2. Inset is simply a zoom in of the first 5 minutes of the x-axis. (C) Relative infectivity of aerosolized Delta variant exposed to increased $[CO_2]$ as a function of time. Note that the errors bars increase with time results from the infectivity of the “Delta, 500 ppm” data set approaching zero which causes the relative standard deviation

to increase. (D) Infectivity of the Delta variant ($\ln([A]/[A_0])$) as a function of time. Least square fit through the Bulk data (R^2 = 0.995). Error bars in all the figures indicate standard error.

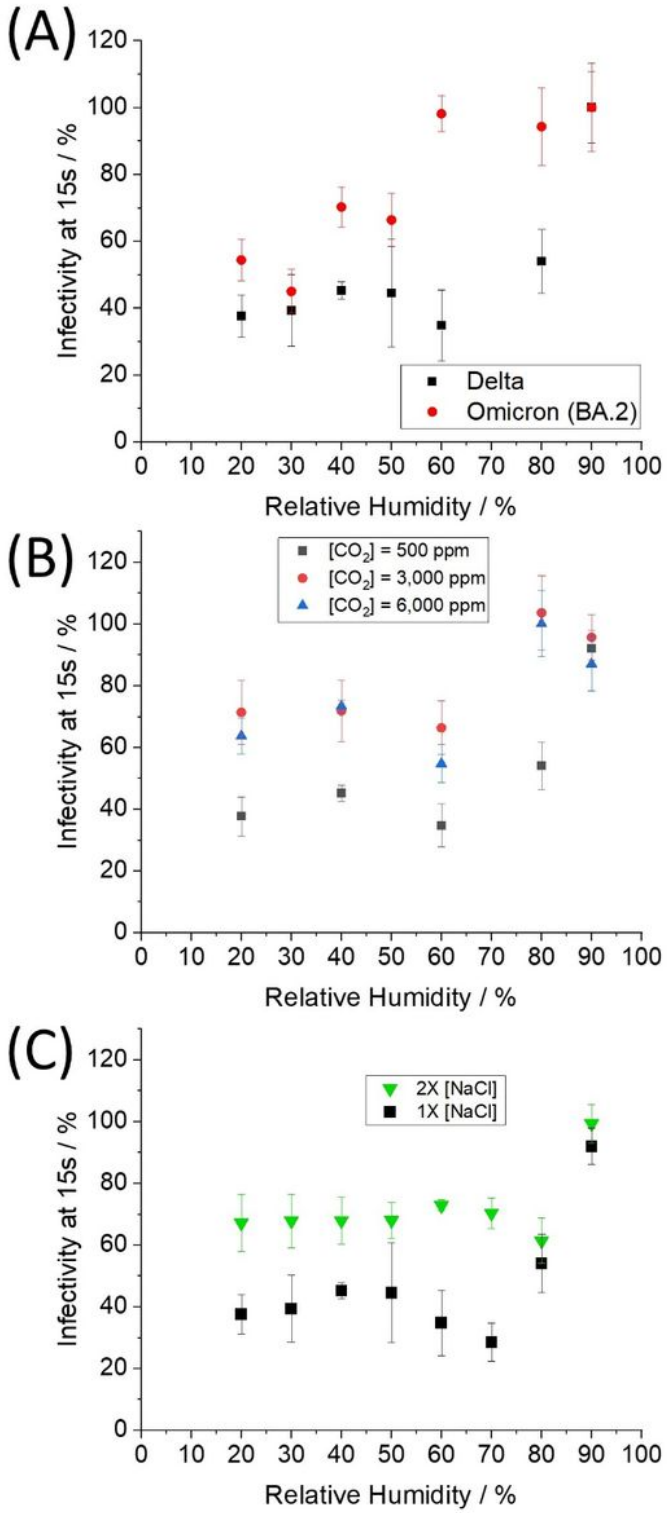

Figure 3

(A) Infectivity of the Delta and Omicron BA.2 variants at 15 seconds in ambient air as a function of relative humidity. Infectivity of the Delta variant at 15 seconds as a function of relative humidity and (B)

[$CO_{2(g)}$] and (C) the [NaCl] in the droplet. Error bars indicate the standard error. A two-way ANOVA of the data in (B) indicated that both CO_2 and RH are significant factors in predicting infectivity, but do not interact, meaning the effect of CO_2 is similar at different RHs (all 80% and below). P-values: RH 0.016, CO_2 <0.0001. A two-way ANOVA of the data in (C) indicated that [NaCl] had a significant effect (P <0.0001), with no significant interaction between the RH and [NaCl].

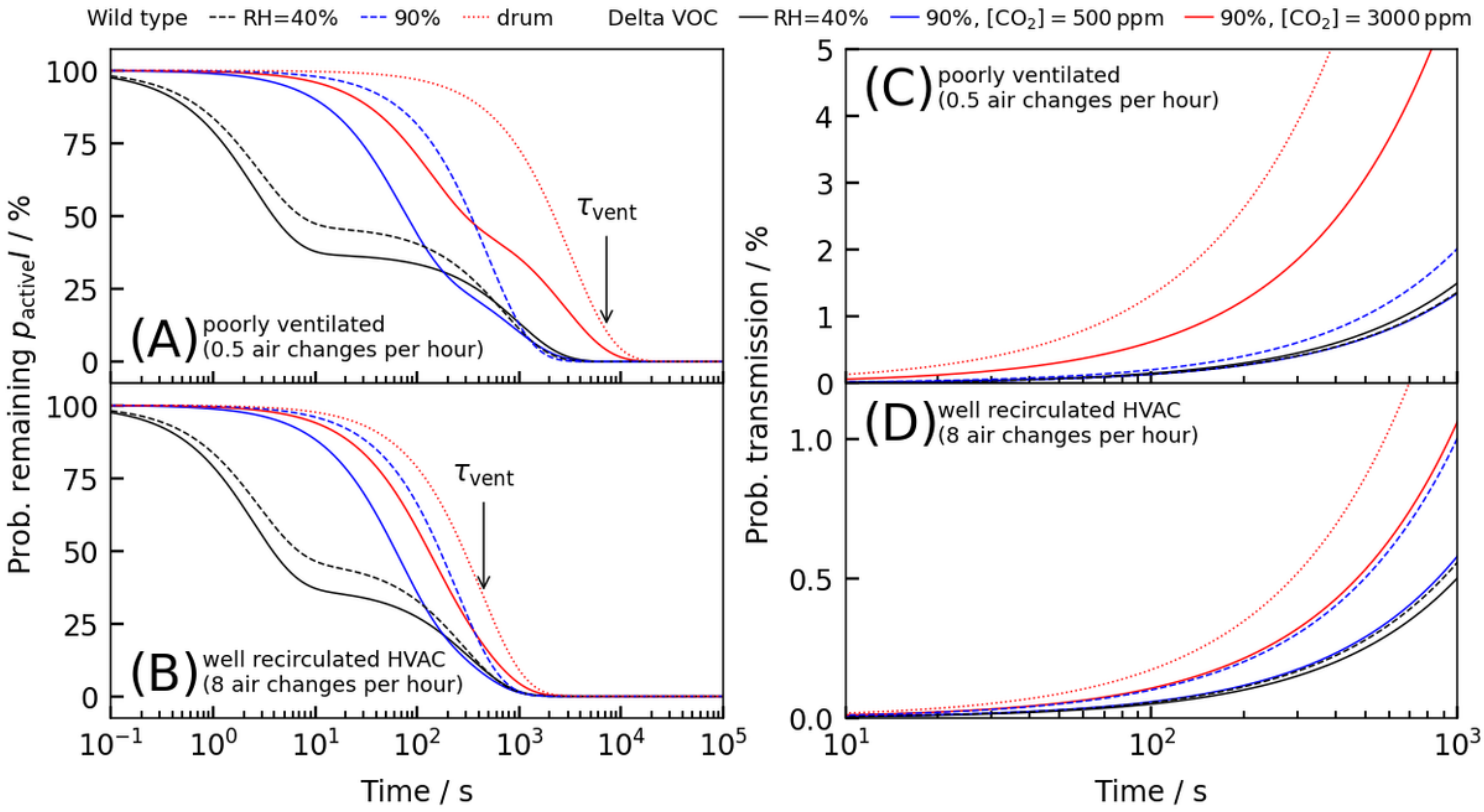

Figure 4

Numerical modelling of risk of indoor transmission in a 300 m^3 classroom that combines fits of infectivity data from Figures 1-3 with the Wells-Riley model for airborne transmission of the Delta VOC in a well-mixed environment. (A-B) Fraction of infectious aerosol particles remaining in the classroom following where “Time” is the time following exhalation of the infectious aerosol. (C-D) Probability of onwards transmission to a susceptible individual assuming a well-mixed environment, where “Time” is the time following occupation of the room. An infectious quanta production rate of 0.1s^{-1} is assumed *(38)*. Decay profile in (A-B) is used to model the transmission risk in (C-D).

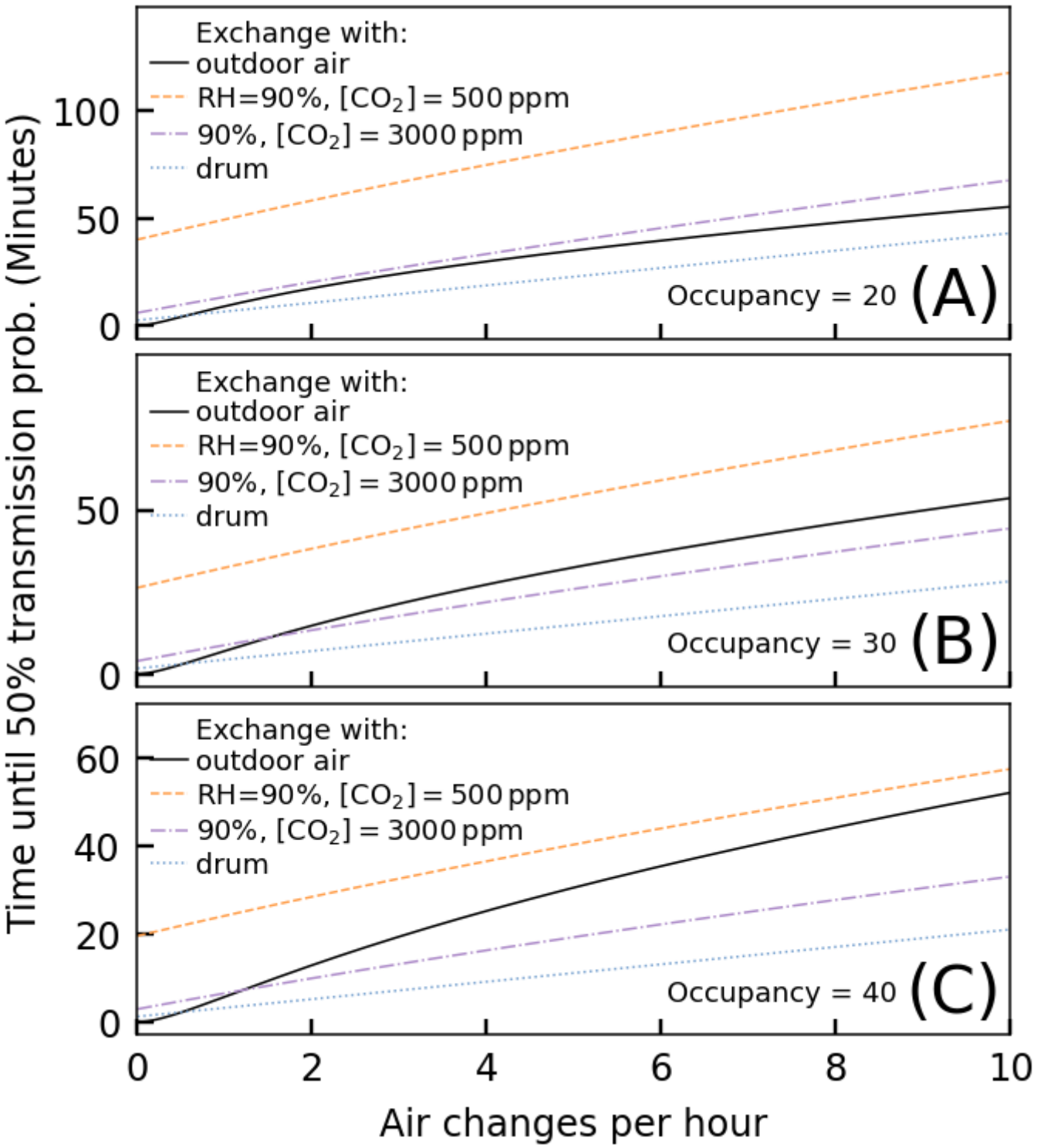

Figure 5

Time until there is a 50% chance that at least one susceptible person will have become infected in an occupied classroom containing a single infected individual, where the viral decay rate is dictated by the RH and $[CO_{2(g)}]$ in the replacement air. We combine estimates of the $[CO_{2(g)}]$ in the room with interpolations of the datasets for Delta variant's infectivity at 90% RH to estimate the risk when exchanging with outdoor air (black, 40% RH, 450 ppm $[CO_{2(g)}]$). This interpolation is purely intended to illustrate the nonlinear role of ventilation qualitatively, and so these numbers should not be taken literally.

For comparison we also show the expectation at fixed low (purple) and high (orange) [$CO_{2(g)}$] without any interpolation; this models recirculation flow within a HVAC system. The number of occupants is varied (A) 20, (B) 30, and (C) 40. An infectious quanta production rate of $0.1s^{-1}$ is assumed.

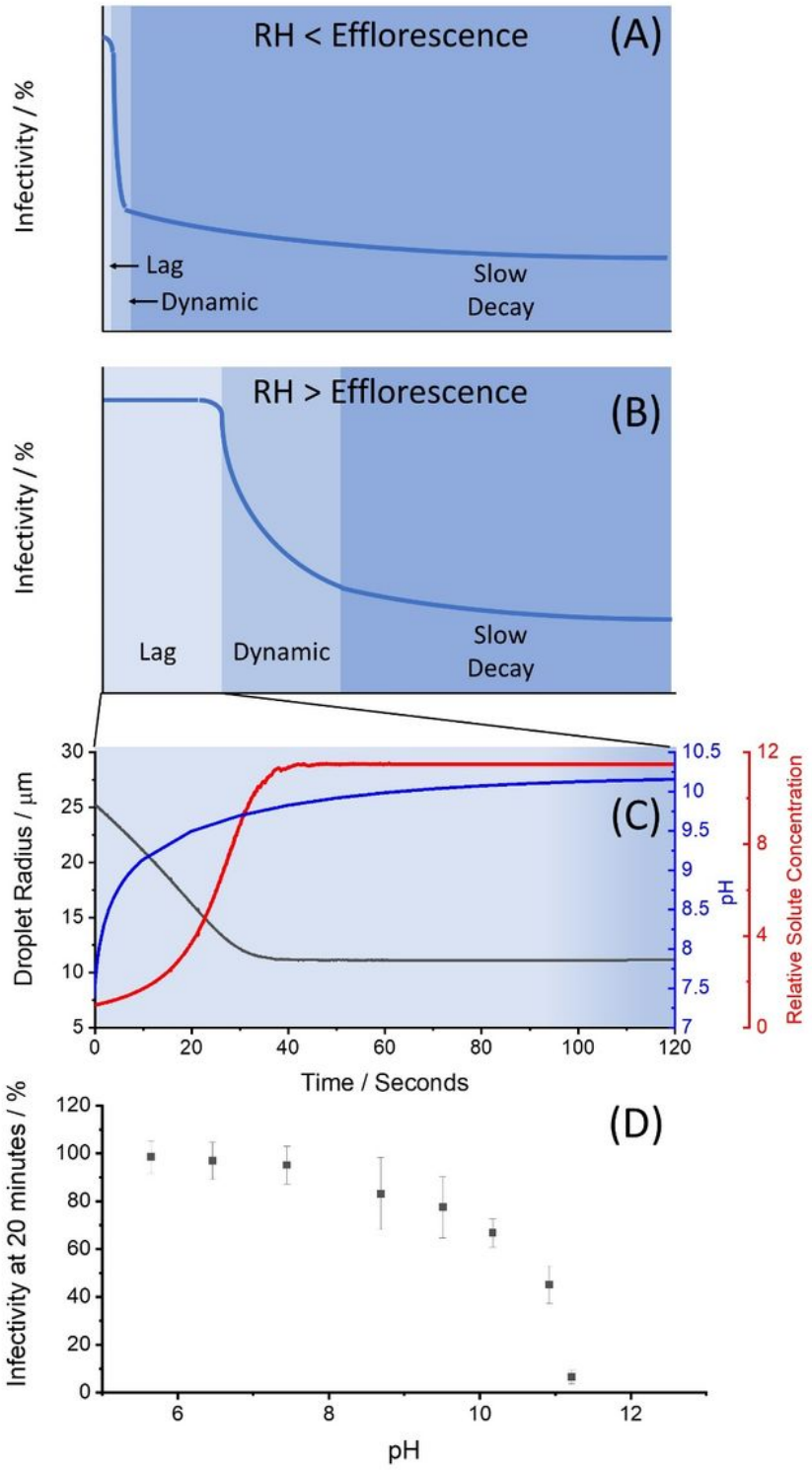

Figure 6

Summary of the Triphasic Viral Aerosol Decay (TVAD) profile of respiratory aerosol, where the general regions are indicated ((A) and (B)) are governed by the conditions in the droplet (Bottom). The three phases are the “Lag Phase”, the “Dynamic Phase” and the “Slow Decay Phase”. Conditions in the droplet (C) are estimates for a respiratory droplet injected into 90% RH at 500 ppm [$CO_{2(g)}$] based upon previously published reports (14, 17). The dynamics of the TVAD are governed by the virus’s sensitivity to pH of the aerosol (D); data from previous study (*14*).

Supplementary Files

This is a list of supplementary files associated with this preprint. Click to download.

- DeltaCO2PaperNatureSupplementalInformationFinal.docx